Nascent fusion pore opening monitored at single-SNAREpin resolution

Paul Heo, Jeff Coleman, Jean-Baptiste Fleury, James Rothman, Frederic Pincet

Nascent fusion pore opening monitored at single-SNAREpin resolution

Paul Heo[a,b], Jeff Coleman[c,d], Jean-Baptiste Fleury[e,f], James E. Rothman[c,d,1], and Frederic Pincet[a,c,d,1]

[a]Laboratoire de Physique de l'Ecole Normale Supérieure, Ecole Normale Supérieure (ENS), Université Paris Sciences et Lettres (PSL), CNRS, Sorbonne Université, Université de Paris, F-75005 Paris, France; [b]Institute of Psychiatry and Neuroscience of Paris, INSERM U1266, F-75014 Paris, France; [c]Department of Cell Biology, School of Medicine, Yale University, New Haven, CT 06520; [d]Nanobiology Institute, Yale School of Medicine, West Haven, CT 06516; [e]Department of Experimental Physics, Saarland University, Saarbruecken D-66123, Germany; and [f]Center for Biophysics, Saarland University, Saarbruecken D-66123, Germany

Contributed by James E. Rothman, December 29, 2020 (sent for review December 4, 2020; reviewed by Nicolas Rodriguez and Thomas H. Soellner)

Vesicle fusion with a target membrane is a key event in cellular trafficking and ensures cargo transport within the cell and between cells. The formation of a protein complex, called SNAREpin, provides the energy necessary for the fusion process. In a three-dimensional microfluidic chip, we monitored the fusion of small vesicles with a suspended asymmetric lipid bilayer. Adding ion channels into the vesicles, our setup allows the observation of a single fusion event by electrophysiology with 10-μs precision. Intriguingly, we identified that small transient fusion pores of discrete sizes reversibly opened with a characteristic lifetime of ∼350 ms. The distribution of their apparent diameters displayed two peaks, at 0.4 ± 0.1 nm and 0.8 ± 0.2 nm. Varying the number of SNAREpins, we demonstrated that the first peak corresponds to fusion pores induced by a single SNAREpin and the second peak is associated with pores involving two SNAREpins acting simultaneously. The pore size fluctuations provide a direct estimate of the energy landscape of the pore. By extrapolation, the energy landscape for three SNAREpins does not exhibit any thermally significant energy barrier, showing that pores larger than 1.5 nm are spontaneously produced by three or more SNAREpins acting simultaneously, and expand indefinitely. Our results quantitatively explain why one SNAREpin is sufficient to open a fusion pore and more than three SNAREpins are required for cargo release. Finally, they also explain why a machinery that synchronizes three SNAREpins, or more, is mandatory to ensure fast neurotransmitter release during synaptic transmission.

membrane fusion | SNAREs | metastable states | suspended bilayer

Intracellular trafficking is a sophisticated communication system that helps maintain cellular, tissue, and organism homeostasis (1, 2). It is largely achieved by the transport of encapsulated cargo inside vesicles from a donor to a target compartment. Fusion of the vesicle with the target membrane induces the release of the cargo through a fusion pore, which is an aqueous channel surrounded by lipids and/or proteins (3). Opening a fusion pore is energetically costly because of the intrinsic membrane physical chemistry; thus it is unable to occur spontaneously under physiological conditions. Hence, proteins are required to provide energy that actively opens the fusion pore, thereby allowing cargo transport. These proteins situated on the vesicle (vSNARE) and the target membrane (tSNARE) were identified more than two decades ago (4). The zippering of the cognate vSNARE and tSNARE into SNAREpins brings the two membranes in close apposition and eventually opens up a fusion pore between the vesicle and the target compartment. The expansion of the fusion pore beyond 2 nm in diameter has been largely studied, both in vivo and in vitro (5–12). However, the efficiency of cargo release is likely to depend on the initial phase of the expansion process, that is, when the pore is below 2 nm. This scenario is only scarcely described in the literature because of technical difficulties required to accurately characterize such small pores. Recent studies based on in vitro electrophysiology approaches have shown the possibility to overcome these limitation1 using nanodisc-based fusion processes (7–11).

Here, we present an in vitro approach and study the initial phase of vesicle fusion by current measurements. Using a three-dimensional (3D) microfluidic chip, we monitored the fusion of small vSNARE-decorated vesicles with a suspended asymmetric membrane containing tSNAREs and having the same lipid composition as a typical plasma membrane. We identified three fusion pore stages: two reversible phases in which the fusion pore has an apparent diameter of 0.4 ± 0.1 nm and 0.8 ± 0.2 nm, and an irreversible phase above 1.5 nm where the fusion pore expands continuously and indefinitely. We further show that these stages can be attributed to the number of SNAREpins engaged in the fusion process, from one to three and more, respectively.

Results

Fusion Pores Are Specifically Opened by the Assembly of Cognate SNAREs. The tSNARE-decorated membrane used to perform the experiments was reconstituted in a microfluidic device we recently developed (Fig. 1 *A* and *B*) (13). Horizontally suspended between two channels, the asymmetric membrane, that is, both lipid leaflets have different compositions, provides a better mimic of the physiological plasma membrane than standard symmetric membranes. The top leaflet, representing the cytosolic side, is composed of DOPC:DOPS:Cholesterol:DOPE:PIP2 at 7:15:45:30:3% in moles, and the bottom one contains DOPC:DOPS:Cholesterol:DOPE:Sphingomyelin at 20:5:45:15:15% in moles to resemble the extracellular leaflet (see *Materials and Methods* for lipid acronyms and details). In brief, a nanoliter squalene droplet is trapped in a 100-μm

Significance

Using our recently designed microfluidic setup, we investigated the early stage of SNAREpin-induced fusion. We discovered the existence of subsecond transient fusion pores with a well-defined subnanometer size that occur when one or two SNAREpins are mediating vesicle fusion. In contrast, when vesicle fusion is mediated by three SNAREpins, the fusion pore reaches a diameter larger than 1.5 nm and expands spontaneously and indefinitely. These results quantitatively explain the need for a complex machinery to ensure a submillisecond neurotransmitter release after the arrival of the action potential during synaptic transmission.

Author contributions: P.H., J.-B.F., J.E.R., and F.P. designed research; P.H. performed research; J.C. contributed new reagents/analytic tools; P.H., J.-B.F., J.E.R., and F.P. analyzed data; and P.H., J.C., J.-B.F., J.E.R., and F.P. wrote the paper.

Reviewers: N.R., Sorbonne University; and T.H.S., University of Heidelberg.

The authors declare no competing interest.

[1]To whom correspondence may be addressed. Email: james.rothman@yale.edu or pincet@lps.ens.fr.

This article contains supporting information online at https://www.pnas.org/lookup/suppl/doi:10.1073/pnas.2024922118/-/DCSupplemental.

Published January 25, 2021.

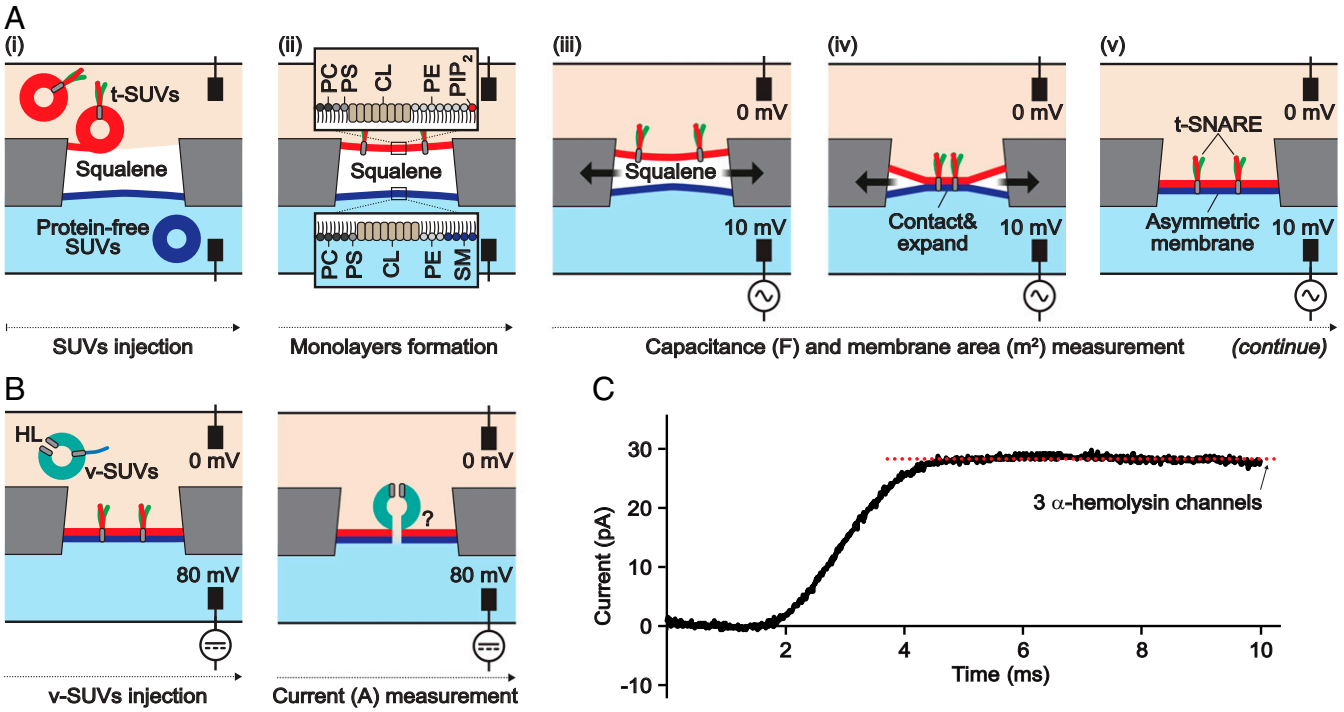

Fig. 1. SNARE-induced pores. (*A*) The tPLM formation. The formation of the tSNARE-decorated plasma-like membrane is described in the five cartoons. (*i*) SUVs are flown in two microfluidic channels that are separated by a hole filled beforehand with a 1-nL squalene droplet. The SUVs spread at the oil/buffer interface in each channel, forming a leaflet on each side of the squalene droplet. Each leaflet has the same composition as the corresponding SUVs. (*ii*) The top leaflet is made of DOPC:DOPS:Cholesterol:DOPE:PIP2 at 7:15:45:30:3% in moles, and the bottom leaflet composition is DOPC:DOPS:Cholesterol:DOPE: Sphingomyelin at 20:5:45:15:15% in moles, resembling the cytosolic and extracellular leaflets of the plasma membrane. In addition, the SUVs circulating in the top channel contained tSNAREs that are also inserted in the leaflet with the desired orientation. (*iii*) The squalene is absorbed by the chip in ~1 h, decreasing, progressively, the interleaflet distance. (*iv*) When a sufficient amount of squalene has been absorbed, the two leaflets contact in the center of the hole and nucleate a bilayer. This nucleation is attested by capacitance measurement (10-mV alternating current). (*v*) Upon completion of squalene absorption, the suspended asymmetric bilayer with tSNAREs is fully expanded and remains stable for more than 3 h. (*B*) Fusion pore observation. The vSNARE-decorated vesicles containing protein channels, α-hemolysin heptamers, (vSUVs) are injected, and a constant 80-mV voltage is applied between the two channels. When vSUV fuses with the tPLM, a fusion pore opens. At that point, the presence of the α-hemolysin channels guarantees the continuity of the aqueous medium between the two channels, and the current can be measured at 100 kHz, directly attesting the opening of the fusion pore. (*C*) Observation of fusion pore opening by current measurement. During the first 2 ms, no current is observed. At 2 ms, a sudden jump in current demonstrates the opening of a fusion pore (red dashed line). Such pore formation is specifically induced by the formation of SNAREpins.

hole separating the two channels that are filled with HK buffer (25 mM Hepes, 150 mM KCl, pH 7.4). First, small unilamellar vesicles (SUVs) having the same composition as the outer leaflet (extracellular monolayer mimic) are flowed in the bottom channel, and tSNARE-reconstituted SUVs (in a ratio one t-SNARE per 400 lipids) with the composition of the inner leaflet (cytosolic monolayer mimic) are injected into the top channel (Fig. 1*A*). These SUVs spontaneously spread at the corresponding squalene/buffer interface, thereby forming a lipid monolayer. Then, the microfluidic chip completely absorbs the squalene droplet in ~1 h, bringing the two monolayers in contact, which creates the suspended bilayer membrane. We previously showed that the tSNAREs embedded in the reconstituted bilayer are active and oriented toward the cytosolic side of the membrane (13). This plasma-like suspended membrane with tSNAREs formed using this protocol will be referred to as tPLM hereinafter.

We use this tPLM as a target membrane to study fusion. Electric measurements are often used to observe single fusion events (5, 14). The conductance of a fusion pore represents the ability of ions to pass through the pore and is a common technique to quantify its size. An accurate value of a membrane's conductance is usually obtained by applying constant voltage across the membrane and measuring the resulting current. However, during the fusion of a small vesicle with a large membrane separating two electrodes, the fused vesicle and the target form a continuous membrane, preventing direct flow of ions between the two sides (5, 14). To circumvent this issue, vesicles have recently been replaced in vitro by small flat membranes, called nanodiscs (7–11). The fusion pore that opens between a nanodisc and the target membrane behaves as a permanently opened channel between the two sides. Here, we propose an alternate solution by inserting three α-hemolysin channels in the membrane of SUVs containing vSNAREs (vSUVs), removing any constraint that may arise from the dimension and geometry of nanodiscs. α-Hemolysin channels are well characterized, both structurally and electrically (13, 15). Another virtue of using vSUVs containing artificial channels is that they do not interfere with the fusion pore formation between vesicle and target membrane (Fig. 1*B*), and let current flow through the pore during the fusion process. In our setup, the vesicle and target membrane fuse with the geometry found in physiological systems, while the channels allow the flow of ions between the two sides (see *Materials and Methods* for details on vSUVs preparations). To check that the addition of α-hemolysin channels in vSUVs did not affect the fusion process, we performed a standard fusion assay in bulk by mixing tSUVs and vSUVs. The overall fusion kinetics were exactly the same with and without α-hemolysin channels (*SI Appendix*, Fig. S1). In the microfluidic setup, these vSUVs were injected in the top channel so that, when a fusion pore opens, ions can flow from one side of the suspended membrane to the other through the fusion pore and the α-hemolysin channels (Fig. 1*B*) (14).

A −80-mV voltage was applied between the two sides of the tPLM, and series of 5-s current measurements separated by 0.5 s for data saving were acquired at 100 kHz. The corresponding current noise of the raw data in the 5-s traces was ∼1 pA, as observed, for instance, in *SI Appendix*, Fig. S2*A*. As expected, sudden current increases were observed when vSUVs containing ∼70 outward facing vSNAREs were injected on the tPLM (Fig. 1*C*). These current jumps typically occurred over a few milliseconds. Then either the current decreased back to zero or remained plateauing for up to several seconds at a few tens of picoamperes. To attest that these current variations were specifically due to the assembly of SNAREpins, we performed several controls: 1) vSUV vs. protein-free suspended membrane, 2) vSUVs vs. tPLM blocked by the cytosolic domain of vSNARE, 3) protein-free SUVs vs. tPLM, and 4) vSUVs without α-hemolysin vs. tPLM. Current increases were not observed in any of these controls. Hence, these current increases clearly represent the opening of a SNARE-induced large fusion pore. The observed current plateau is the result of the α-hemolysin channels. Indeed, initially, the flow of ions is limited by the nascent fusion pore size. However, when the fusion pore expands, the α-hemolysin channels shield the measurement of current signal and prevent the accurate monitoring of large pores. The plateau value indicates the number of α-hemolysin channels in the vSUVs and determines the observation window for fusion pore formation. Under our experimental conditions, each α-hemolysin channels contribute to a ∼10-pA current flow when the fusion pore is expanded (see *Materials and Methods*). In the example displayed in Fig. 1*C*, the plateau current, of ∼30 pA, is indicative of three α-hemolysin channels in the fusing vSUV. The majority of vSUV we observed contained two to five α-hemolysin channels, but we observed extreme cases with one (*SI Appendix*, Fig. S2*A*) or eight channels (*SI Appendix*, Fig. S2*B*). The conditions described here are sufficient to measure initial kinetics of the pore, typically up to 1 nm to 2 nm, independently of the number of α-hemolysin channels in the vSUV (as detailed in *SI Appendix*, Fig. S3 and *Supplementary Text*).

Formation of Transient Fusion Pores Correlated with the Number of SNAREpins. Monitoring the initial kinetics of pore formation and detecting small size fusion pores requires a reduction of the current noise. Either by performing a 10-point rolling average or by cutting frequencies above 10 kHz, noise was reduced down to 0.2 pA to 0.3 pA. This strategy reduces the time resolution to ∼100 μs. Through this filtering, we discovered that many small transient pores frequently opened and closed in the membrane. These transient pores were not observed in the control experiments, attesting that they were caused by SNAREpin formation. Strikingly, the conductance of each transient fusion pore remained at a well-characterized plateau value (Fig. 2*A*), and sometimes several plateau values were observed on the same pore (Fig. 2*B*).

To characterize the transient pores, we determined the average plateau value of the current of the 79 transient pores we identified. When plotting the distribution of these plateau values, surprisingly, two distinct peaks emerged (Fig. 2*C*). An alternate visualization of this distribution and these peaks is to plot the pore size. First, the notion of size of the pore needs to be explicitly explained. The fusion pore is often viewed as a cylindrical tube. With this geometry, the conductance is proportional to the square of the diameter of the pore (see *Material and Methods* for details on the calculation of the pore diameter). This relationship between the conductance and the diameter of the tube has frequently been used. The same procedure will be used to analyze our measurements, and the size of a pore will be defined as the diameter of a 10-nm-long tube having the same conductance as the pore. We plotted the distributions of the mean diameters corresponding to the observed currents (Fig. 2*D*). These mean diameters range between 0.3 nm and 0.5 nm for the

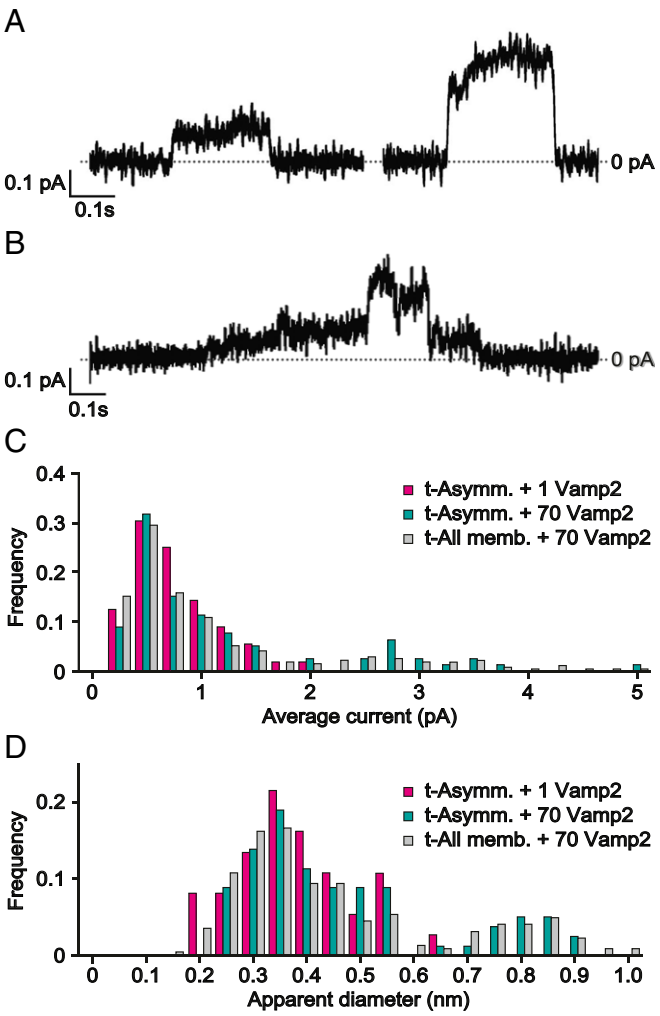

Fig. 2. Transient fusion pores. (*A*) Two metastable states. Two types of transient pores with discrete dimensions were observed. Typical current traces are presented for the smallest (left) and largest (right) pores. (*B*) Cycling between the two states. Example of a pore opening in the small transient state before transitioning to the larger state and cycling back to the small state before resealing. (*C*) Mean current. Histogram representing the distribution of the mean value of the current of vesicles forming a single SNAREpin (pink, 56 pores), vesicles with 70 vSNAREs fusing on the tPLM (green, 79 pores), and vesicles with 70 vSNAREs fusing on tPLM or asymmetric membranes (gray, 222 pores). (*D*) Mean apparent diameter. The distribution of the pore's mean apparent diameter is presented with the same color coding as in *C*.

first peak and between 0.7 nm and 1 nm for the second peak. The mean apparent pore diameters are 0.4 ± 0.1 nm and 0.8 ± 0.2 nm, for the first and second peaks, respectively. These small dimensions of the transient pores, commensurate with ion sizes, make the actual molecular nature of the pore difficult to determine. Is it the usual representation with a tubular shape or does it resemble a defect between the two adjoining membranes through which ions can be carried? Our study cannot establish it. Hence, for the sake of clarity, we will continue to define the size of the fusion pore as the "apparent diameter" of a cylindrical tube having the same conductance.

We first tested whether the two peaks were specific to the asymmetric membrane. As a comparison, we made a symmetric membrane having the compositions previously used in nanodisc experiments (DPhPC:DOPS:DOPE at 54:16:30% in moles) and a symmetric membrane having the composition similar to that

of the "cytosolic" leaflet (DOPC:DOPS:Cholesterol:DOPE at 10:15:45:30% in moles). We found no significant difference in the current and pore diameter distributions measured with an asymmetric, or a symmetric, membrane (Fig. 2 *C* and *D*).

Next, we hypothesized that each discrete size fusion pore corresponds to a precise number of acting SNAREpins. To test this hypothesis, we performed similar experiments with vSUV having, on average, less than 1 vSNARE facing outward. In this set of experiments, fusion events with pores larger than 1.5 nm, such as the ones observed with 70 vSNAREs per SUV, completely disappeared. Only one transient fusion pore out of the observed 61 was part of the second peak, the others forming the first peak. This is consistent with a stochastic distribution of the vSNAREs; rarely, two vSNAREs are present and simultaneously acting to open the fusion pore. This result confirms that transient pores having a conductance in the first peak can be attributed to the action of a single SNAREpin, while the second peak corresponds to transient pores opened by the simultaneous action of two SNAREpins. Flickering of a transient pore between two states as in Fig. 2*B* indicates transitions between one and two simultaneously acting SNAREpins. The reverse transition from two to one acting SNAREpin indicates that one of the SNAREpins became inactive. Two origins can be envisioned for the deactivation of a SNAREpin: disassembly or complete assembly. Spontaneous disassembly of a SNAREpin is energetically impossible on the experimental time scale (16). Hence, the disassembly cannot explain the reverse transition. The most likely explanation is that one of the transmembrane domains flipped across the pore and is followed by complete assembly of the SNAREpin. After this crossing of the pore, both transmembrane domains are on the same side of the fusion pore, making SNAREpin zippering mechanically inefficient to keep the nascent pore open and allowing complete zippering of the SNAREpin which, as a result, becomes inactive.

Energy Involved in the Prefusion Pore Opening and SNARE Energy Contribution. In this section, we are trying to derive the energy landscape of each of the intermediate pores from the fluctuations of the apparent diameter. Hence, we need to focus on the instantaneous data points, not on the mean values that are presented in Fig. 2 *C* and *D*. Also, because of the logarithmic dependency of the energy on the number of data points, we decided to pool together all the observed transient pores from both asymmetric and symmetric membranes to obtain the best possible statistics. The histograms of the instantaneous apparent diameter are provided in Fig. 3*A*. These distributions contain ~2 million data points for the transient pores generated by a single SNAREpin and ~600,000 data points for the ones created by two simultaneously acting SNAREpins. Since thermal fluctuations are responsible for the variations in pore dimensions (see *SI Appendix, Supplementary Text* for detailed calculation), it is possible to directly derive the energy landscape of each type of pore in the diameter range between 0.1 and 0.9 nm for the single-SNAREpin–induced pore and between 0.4 and 1.5 nm for the two-SNAREpin–induced pore (Fig. 3*B*; see *Material and Methods* for details). In the overlapping regions of these size ranges, that is, pore diameters between 0.4 and 0.9 nm, it is possible to establish the contribution of one SNAREpin by subtracting the energy landscapes (Fig. 3*C*). The resulting slope provides an energy of ~20 k_BT per nanometer of apparent diameter. Here, the SNAREpin is acting along the rim of the pore, meaning it is a line actant that generates a force resembling a negative line tension. In this line tension-based model, the energy variation of the pore is equal to the product of a line tension and the length of the rim. Thus, for a tube-like pore, a single SNAREpin generates a negative line tension of ~25 pN (*SI Appendix, Supplementary Text*). The fact that at least three SNAREpins are required to expand the fusion pore suggests that the equivalent fusion pore line tension is ~50 pN to 75 pN, which is of the same order as the line tension of a hole in the membrane (17) and as the value previously predicted by simulations for SNARE and influenza-mediated

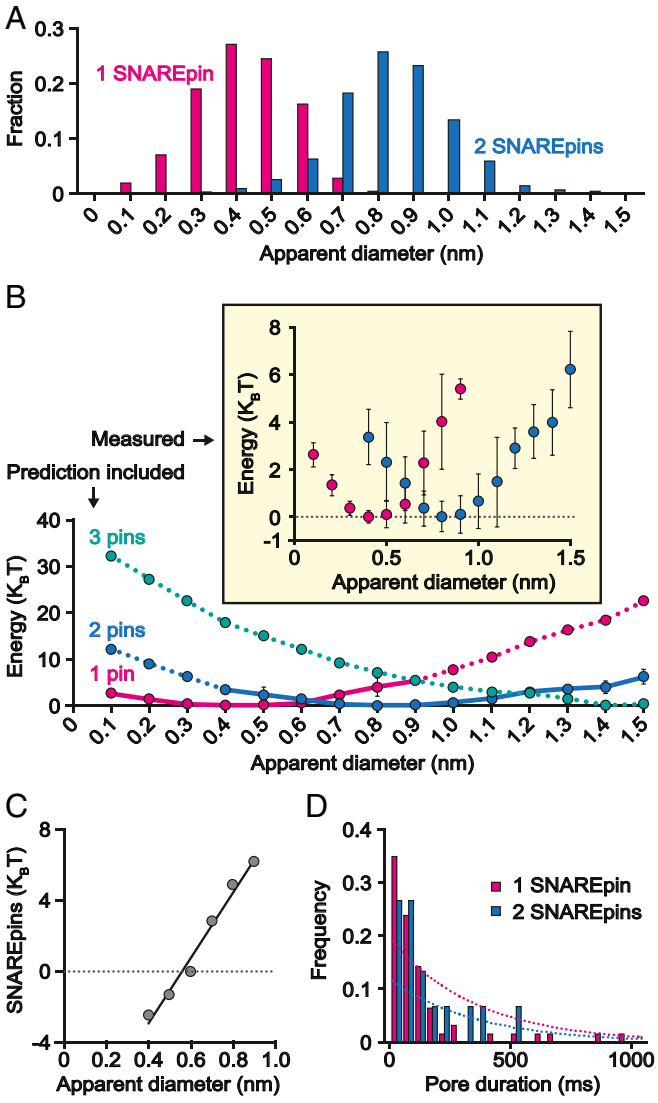

Fig. 3. Energetic characterization of the transient fusion pore. (*A*) Instantaneous apparent diameter. Histogram representing the distributions of the instantaneous apparent diameter for the small pore (0.4 nm, ~2 million values, pink) and the large pore (0.8 nm, ~0.6 million values, blue). (*B*) Energy landscapes of the pores. The measured energy landscapes of the small (pink line in the main panel and pink data points in the inset) and large (blue line in the main panel and blue data points in the inset) pores are calculated as indicated in *Materials and Methods*. The error bars are SEs. Adding the contribution of a single SNAREpin to the energy landscapes from the measured data provides the extension of the energy landscapes with one (pink dashed line in the main panel) and two (blue dashed line in the main panel) SNAREpins over the whole range between 0.1 and 1.5 nm and direct prediction of the energy landscape with three SNAREpins (green dashed line in the main panel). See *Materials and Methods* for details. Note that all the energy landscapes are defined with an arbitrary offset (zero at the energy minimum) and cannot be absolutely compared. Only the relative variations are relevant. (*C*) Contribution of a single SNAREpin. The difference in energy landscape between the small and large transient pores is due to the energy provided by a single SNAREpin. This difference is presented with an arbitrary offset in energy (zero at 0.6 nm). The slope is the contribution of a single SNAREpin: ~20 k_BT per nanometer of apparent pore diameter. (*D*) Distribution of the small (pink) and large (blue) pore duration. The characteristic times obtained by fitting the histograms are the same for both types of pores: ~350 ms.

fusion pores (18, 19). Since we do not know the actual geometry of the pores, these line tension values can only be considered as approximate but provide an idea of the forces involved in the initial expansion process.

To understand why we observe exactly two types of transient fusion pore and not three or more, we can use the contribution of a single SNAREpin and add it to the energy landscape of the larger transient pore generated by two SNAREpins. The resulting energy landscape, which is a prediction of the behavior of a pore opened by three SNAREpins, does not display any significant energy barrier, indicating that the fusion pore will indefinitely expand. Hence, our results also show that any pore larger than 1.5 nm is necessarily triggered by at least three SNAREpins and will irreversibly expand.

Discussion

Mean Lifetime of the Fusion Pore and Kinetics of Spontaneous SNAREpin Synchronization. The transient fusion pore durations display similar distributions, with a characteristic time of ∼350 ms when induced by one or two SNAREpins (Fig. 3*D*). Two origins can be envisioned for pore closure. First, it may be spontaneous thermal fluctuations that just reseal the pore. The lifetime of a metastable state in an energetically activated process can be approximately expressed as $\tau_0 e^{E_b/k_BT}$, where $\tau_0 \approx 1$ ns, and E_b is the activation energy (20–22). Hence, energetically, a 350-ms lifetime of the pore would indicate a resealing energy barrier of $\sim 20\ k_BT$, which is reasonable in regard to the activation energy for fusion ($\sim 30\ k_BT$). Second, just like for the transition from two to one acting SNAREpin mentioned in *Results*, the active SNAREpins may become inactive by flipping the transmembrane domain of vSNARE or from Syntaxin1A across the pore. When such an event occurs, the two transmembrane domains end up on the same side of the pore, which prevents any mechanical action of the SNARE complex to maintain the pore open. In this scenario, it would be expected that the larger transient pores (0.8 nm), induced by two SNAREpins, close by transiting through the smaller one (0.4 nm) due to a single SNAREpin. However, in most cases, resealing occurred in one step, as in the example displayed in Fig. 2*A*. We rarely observed 0.8-nm pore closing in a stepwise manner by pausing in the intermediate 0.4-nm-diameter state, such as shown in Fig. 2*B*. These observations may seem to favor the first explanation for pore resealing, that is, thermal fluctuations. However, it is plausible that some convective flows within the membrane and/or protein interactions may facilitate collective inactivation of both SNAREpins. Hence, we cannot favor one origin over the other with our current results; possibly, both types of resealing may sequentially occur with the same SNAREpin.

The lifetime of the transient fusion pores also provides information on the spontaneous synchronization of the SNAREpins. Initially, only one SNAREpin is formed and starts pulling the membranes together to open the fusion pore. Then, two different events can occur: Either a pore opens or a second SNAREpin spontaneously synchronizes to promote pore opening. In our experiments, we observed both events, with 4 times more occurrences when the fusion pore is induced by one SNAREpin. This observation indicates that the assembly and synchronization of a second SNAREpin takes, on average, ∼4 times longer than pore opening triggered by one SNAREpin. It was previously observed that fusion pore opening takes ∼1 s with a single SNAREpin. Hence, under the conditions we used, the spontaneous assembly and synchronization of the second SNAREpin requires a few seconds, on average. This relatively long delay is primarily due to the time required for two cognate SNAREpins to meet and start assembling. It will depend on the experimental conditions, for example, SNARE density, mobility, or orientation.

Lipid Mixing Can Be Achieved by One SNAREpin, but Three SNAREpins Are Required for Efficient Cargo Release. We and others previously established that one or two SNAREpins are sufficient to open the fusion pore, as attested by membrane lipid mixing, but not to keep it sufficiently open to fully release the cargo encapsulated in the fusing vesicle (23–26). Here, the pores we monitored were either small transient pores or large pores corresponding to full fusion having three or more SNAREpins simultaneously. Hence, the results presented here strikingly correlate with our previous observation and may explain why three SNAREpins are necessary: The transient fusion pores opened by one or two SNAREpins are too small for efficient cargo release (see discussion below). We will test this hypothesis.

Each open/close cycle of the fusion pore may induce a burst of lipid mixing in the tPLM and cargo release in the extracellular-like side. Lipid mixing and cargo release can be evaluated, as we know the size and lifetime of a pore, which are sufficient to predict the kinetics of lipid mixing and cargo release. Assuming free diffusion along the pore, the characteristic times of both processes can be estimated (*SI Appendix*, *Supplementary Text*). In two dimensions, the characteristic time for lipid mixing, τ_l, can be written as $\tau_l = Lr_v^2/2D_l r$, where L is the pore length, r_v is the vesicle radius, D_l is the lipid diffusion coefficient, and r is the pore radius. Using typical values for these parameters, $\tau_l \approx 20$ ms for a 0.4-nm pore, and $\tau_l \approx 10$ ms for a 0.8-nm pore (*SI Appendix*, *Supplementary Text*). These values are smaller than the typical 350-ms lifetime of the transient pores, showing that lipid mixing is achieved as soon as the first fusion pore opens. Hence, a single lipid mixing burst is expected when the first pore opens. Because τ_l is much smaller than the lifetime of the pore, complete lipid mixing is achieved when this first pore opens. When subsequent pores appear, the vSUV and tPLM already have the same lipid composition, and there is no more apparent lipid mixing: Lipids are exchanged, but the compositions remain unchanged. This analysis of the time for lipid mixing is corroborated by the transfer of α-hemolysin to the PLM. Since the typical diffusion coefficient of transmembrane proteins is 10 to 100 times smaller than that of lipids, α-hemolysin is expected to cross the pore 10 to 100 times slower than lipids; thus it is possible that an α-hemolysin channel reaches the bilayer during the pore lifetime. This crossing was observed. When using vSUVs containing a single vSNARE, we found that the background current remained null for several fusion events before starting to increase, indicating the presence of α-hemolysin channels in the PLM and confirming the slow release of α-hemolysin through the fusion pore.

Similarly, the characteristic time for cargo release, τ_c, is $\tau_c = 4Lr_v^2/[3D_c(r - r_c)^2]$, where D_c is the cargo diffusion coefficient and r_c is the cargo hydrodynamic radius. For a small cargo ($r_c = 0.35$ nm), there is no release through a 0.4-nm pore because the pore is smaller than the molecule size, and $\tau_c \approx 1.5$ s through a 0.8-nm pore, which is larger than the pore lifetime. Hence, no significant cargo release is predicted until a large fusion pore occurs. According to these results, we predict that cargo can only be released when the pore is expanded, that is, when three SNAREpins or more are acting. This confirms our hypothesis and explains what we previously observed: One SNAREpin is sufficient to open the fusion pore, as attested by lipid mixing, but three SNAREpins are needed for efficient cargo release.

Synchronizing SNAREpins for Fast Evoked Release in Synaptic Transmission. The necessity to have three SNAREpins acting simultaneously raises the question of what happens physiologically. Cargo needs to be released in cellular trafficking. The presence of dozens of vSNAREs guarantees that full fusion will eventually occur once a vesicle is docked. In the case of synaptic transmission, it is critical that neurotransmitter release occurs less than 1 ms after the arrival of the action potential. Hence, three SNAREpins need to be synchronized

to expand the nascent fusion pore. This explains why a complex and reliable machinery must be set in place to prime the vesicle by the partial formation of SNAREpins that are synchronously released when needed. This machinery primarily involves Synaptotagmin proteins that block several SNAREpins in a half-zippered state and ensure their synchronous release upon action potential arrival (27).

Our results show that the fusion process can actually be separated into two distinct phases: the opening of the nascent fusion pore and the expansion of the pore for neurotransmitter release. Both phases must occur quickly. We previously predicted that a nascent fusion pore is open with the required speed only when three to six SNAREpins are involved (28). Fewer than three SNAREpins are not sufficient to overcome the energy barrier for fusion in the required time. Conversely, more than six SNAREpins actually slow down fusion even though enough potential energy is stored in the protein assembly process. This counterintuitive result arises from the difficulty of synchronizing all the SNAREpins collectively.

Here, we present an additional constraint, which is that at least three SNAREpins must be simultaneously acting on the nascent pore to expand it after it opens. This constraint narrows the range of initially synchronized SNAREpins toward the upper limit of five or six SNAREpins. Indeed, we saw that pores can fluctuate between one or two simultaneously acting SNAREpins. This observation demonstrates that synchronization of SNAREpins can be altered during the pore opening process. If three SNAREpins were synchronized in the first phase (opening the nascent fusion pore), there is no guarantee that this synchronicity would not be lost during the second phase, that is, pore opening. Hence, to optimize fast neurotransmitter release physiologically, it is more favorable to have the maximum possible number of synchronized SNAREpins. We therefore predict that, optimally, six SNAREpins should be preformed in the primed state; recent experimental observations tend to confirm this prediction (29).

Materials and Methods

Lipids and Acronyms. All lipids were purchased from Avanti Polar Lipids: 1,2-dioleoyl-sn-glycero-3-phosphocholine (Cat. 850375, DOPC), 1,2-dioleoyl-sn-glycero-3-phospho-L-serine (Cat. 840035, DOPS), Cholesterol (Cat. 700000), 1,2-dioleoyl-sn-glycero-3-phosphoethanolamine (Cat. 850725, DOPE), Sphingomyelin (Cat. 860062), L-α-phosphatidylinositol-4,5-bisphosphate (Cat. 840046, PIP2), 1,2-diphytanoyl-sn-glycero-3-phosphocholine (Cat. 850356, DPhPC), and 1,2-dioleoyl-sn-glycero-3-phosphoethanolamine-*N*-(7-nitro-2-1,3-benzoxadiazol-4-yl) (Cat. 810145, NBD-PE).

Microfluidic Device Fabrication. Detailed procedures can be found in previous literature (13). In brief, two molds providing a bottom and top groove with a cylindrical hole (100 * 100, H * ø) were printed using a stereolithography/digital light processing-type 3D printer. After mold assembly, polydimethylsiloxane (PDMS) was poured on it and cured in a 72 °C oven for 50 min. PDMS was detached from the mold and briefly washed using acetone and isopropanol, and postcured in a 72 °C oven overnight. The top groove was sealed with a PDMS slab containing an inlet and an outlet channel to complete the top channel. Another PDMS slab was attached to one side of the bottom channel using liquid PDMS, and, after curing, the slab was punched with a 0.5-mm puncher to create a bottom inlet channel. The other side of the channel was also punched to create a bottom outlet. The bottom groove was sealed with a coverslip using a plasma cleaner to make a bottom channel. After incubation of this device in a 72 °C oven overnight, a quality check of the chip was performed by observing the absorption of the squalene, using a microscope and a patch amplifier (13, 30).

SNAREs and α-Hemolysin Reconstitution into Small Unilamellar Vesicles. The tSNARE (preassembled Syntaxin1A and SNAP25) and vSNARE (VAMP2) were purified following the previously established protocol (31). Hemolysin was purchased from Sigma Aldrich (Cat. H9395). The tSNARE and vSNARE together with hemolysin were reconstituted into SUVs by following a comicellization protocol (32). In brief, tSNARE (400:1 lipid to protein [LP] ratio) and HK buffer (25 mM Hepes, 150 mM KCl, pH7.4) were poured on the lipid film containing DOPC:DOPS:Cholesterol:DOPE:PIP_2 (10:12:40:35:3 mol%) by keeping the 1% octyl-β-d-glucopyranoside (OG) concentration. After dilution with HK buffer two times, the mixture was dialyzed overnight with SM2 bio-bead (BioRad) to remove OG. Then the density gradient medium (OptiPrep, Cat. D1556 in Sigma Aldrich) along with ultracentrifugation were used to collect the tSUVs. The procedure to make vSUVs containing hemolysin channels was the same as above, except for differences in the lipid composition (DOPC:DOPS:Cholesterol:DOPE, 40:10:25:25 mol%) and LP ratio (200:1 for vSNARE, 400:1 for α-hemolysin). No loss of α-hemolysin was observed during the vSUV fabrication process (*SI Appendix*, Fig. S2). To determine the appropriate number of α-hemolysin channels, we considered the following. If the total channel dimensions are smaller than the fusion pore, they will limit the current; thus, it is preferable to have several channels in each SUV. However, too many channels may alter SUV properties. Since each channel has a diameter of ~1.5 nm, we chose to insert, on average, approximately three α-hemolysin channels per vSUV.

Outer Leaflet-Mimicking SUV Preparation. Lipid film containing DOPC:DOPS:Cholesterol:DOPE:Sphingomyelin (20:5:40:15:20 mol%) was hydrated with HK buffer and sonicated in a 12-min cycle of 2 s pulse/2 s pause.

Asymmetric Membrane Containing tSNARE Formation in the Microfluidic Device. Initially, the chip was filled up with squalene. Then ~2 mL of outer leaflet-mimicking SUVs (respectively, tSUVs) was injected into the bottom (respectively, top) channel. They spontaneously fused on the water–oil interfaces, facing top and bottom aqueous phases, of a 1-nL squalene droplet and formed two different monolayers: tSNAREs containing monolayer adjacent to the top channel and protein-free monolayer adjacent to the bottom channel. PDMS continuously absorbed squalene for 1 h, and this procedure facilitated joining the two monolayers from the center to the rim of the cylindrical hole. Membrane formation was observed spontaneously using microscope and patch amplifier, and the membrane area was linearly correlated with the membrane capacitance. Typical membrane lifetime was 4 h. Membrane asymmetry was confirmed by adding 1% of NBD-PE in one of monolayers and observing the quenching effect by flowing dithionite sequentially (13). Orientation of tSNAREs was confirmed using a fluorescent antibody that binds cytosolic domain of synatxin1a.

Fusion Pore Measurement. When the capacitance of tPLM reached a plateau, vSUVs containing hemolysin channels (1 mM lipid concentration) were injected into the top channel. Membrane voltage was clamped to −80 mV, and the current was measured at 100 kHz in the cycle of 5 s measurement and 0.5 s pause (30). Typically, the current was measured for ~30 min. Data were collected until the permanent background increase due to many hemolysins on tPLM after several fusion events.

Data Analysis.

Detection of the small pores. The typical noise in the raw current data was ~1 pA. To detect the small nascent fusion pores, we chose to perform two separate procedures: a rolling average over 10 traces and filtering by removing the frequencies around 50 Hz, that is, the standard frequency of alternating current in Europe, and above 10 kHz. The two resulting and independently obtained sets of traces display a typical noise of ~0.2 pA to 0.3 pA for the initial 5-s traces. After several fusion pores have opened, some α-hemolysin channels have diffused in the tPLM. Their conformation fluctuates slightly, and sometimes they display opening/closing cycles. These fluctuations increase the background noise to a level that is unacceptable for the detection of small pores. Hence, when the noise increased above 0.3 pA, we disregarded the subsequent 5-s traces.

Once the two sets of traces were obtained, sequences in which the current was higher than 1 pA for 2 ms or higher than 0.3pA for 5 ms were automatically detected by a homemade MatLab script. Then, we manually analyzed these events to verify they actually correspond to fusion pores, that is, to remove the small electric glitches that can occur and that are often characterized by positive currents followed by unrealistic negative currents.

Derivation of the pore diameter from the measured current. To obtain the apparent pore diameter, we used α-hemolysin as a reference. With the HK buffer, we measured that the conductance of hemolysin is 0.125 nS. Hence the current passing through a α-hemolysin channel is I_h = 10 pA. Since the conductance is proportional to A/l, where A and l are the channel inner area and length, respectively, the apparent diameter of the pore is

$$d_{ap} = 2\sqrt{l_{ap} l_{ap} A_h / l_h \pi l_h},$$

with $A_h = 1.8\ \text{nm}^2$ and $l_h = 10$ nm for α-hemolysin. Assuming the pore length is the thickness of two bilayers, $l_{ap} \approx 10$ nm $= l_h$. Thus, the value of the apparent diameter we present in the manuscript is $d_{ap} = 2\sqrt{l_{ap} A_h / l_h \pi}$. Note that, as always, there is a proportionality coefficient between the apparent pore diameter and the actual absolute diameter. This mismatch is due to the unknown in the length and actual shape of the pore and is standard in the field. However, this proportionality coefficient is close to 1, so the values are not far from reality, and, importantly the variations of diameter are relatively correct.

Calculation of the energy landscapes. The distributions of instantaneous apparent diameters presented in Fig. 3*A* contain 0.1-nm bins. Calling f_i the fraction of pore diameters in bin i, and f_{max} the maximum of these fractions, the energy for the apparent diameter i is $-k_BT \ln(f_i/f_{max})$, where k_BT is the thermal energy. The results for both pore sizes are presented in Fig. 3*B*.

Data Availability. All study data are included in the article and/or *SI Appendix*.

ACKNOWLEDGMENTS. This work was supported by a European Research Council funded grant under the European Union's Horizon 2020 research and innovation program (Grant Agreement 669612) to J.E.R. and F.P. and by Grant ANR-14-1CHN-0022-01 (to J.E.R.). J.-B.F. acknowledges funding from SFB1027 (Deutsche Forschungsgemeinschaft). We are grateful to Prof. Thomas Söllner, who first suggested the use of protein channels to probe fusion with current measurements.

1. R. Jahn, T. Lang, T. C. Südhof, Membrane fusion. *Cell* **112**, 519–533 (2003).
2. R. Jahn, T. C. Südhof, Synaptic vesicles and exocytosis. *Annu. Rev. Neurosci.* **17**, 219–246 (1994).
3. T. Wang, L. Li, W. Hong, SNARE proteins in membrane trafficking. *Traffic* **18**, 767–775 (2017).
4. T. Weber *et al*., SNAREpins: Minimal machinery for membrane fusion. *Cell* **92**, 759–772 (1998).
5. L. J. Breckenridge, W. Almers, Currents through the fusion pore that forms during exocytosis of a secretory vesicle. *Nature* **328**, 814–817 (1987).
6. J. Hartmann, M. Lindau, A novel Ca^{2+}-dependent step in exocytosis subsequent to vesicle fusion. *FEBS Lett.* **363**, 217–220 (1995).
7. H. Bao *et al*., Dynamics and number of trans-SNARE complexes determine nascent fusion pore properties. *Nature* **554**, 260–263 (2018).
8. D. Das, H. Bao, K. C. Courtney, L. Wu, E. R. Chapman, Resolving kinetic intermediates during the regulated assembly and disassembly of fusion pores. *Nat. Commun.* **11**, 231 (2020).
9. Z. Wu *et al*., Nanodisc-cell fusion: Control of fusion pore nucleation and lifetimes by SNARE protein transmembrane domains. *Sci. Rep.* **6**, 27287 (2016).
10. Z. Wu, S. Thiyagarajan, B. O'Shaughnessy, E. Karatekin, Regulation of exocytotic fusion pores by SNARE protein transmembrane domains. *Front. Mol. Neurosci.* **10**, 315 (2017).
11. N. R. Dudzinski, Z. Wu, E. Karatekin, A nanodisc-cell fusion assay with single-pore sensitivity and sub-millisecond time resolution. *Methods Mol. Biol.* **1860**, 263–275 (2019).
12. C. W. Chang, C. W. Chiang, M. B. Jackson, Fusion pores and their control of neurotransmitter and hormone release. *J. Gen. Physiol.* **149**, 301–322 (2017).
13. P. Heo *et al*., Highly reproducible physiological asymmetric membrane with freely diffusing embedded proteins in a 3D-printed microfluidic setup. *Small* **15**, e1900725 (2019).
14. M. Lindau, W. Almers, Structure and function of fusion pores in exocytosis and ectoplasmic membrane fusion. *Curr. Opin. Cell Biol.* **7**, 509–517 (1995).
15. R. Stefureac, Y. T. Long, H. B. Kraatz, P. Howard, J. S. Lee, Transport of alpha-helical peptides through alpha-hemolysin and aerolysin pores. *Biochemistry* **45**, 9172–9179 (2006).
16. Y. Gao *et al*., Single reconstituted neuronal SNARE complexes zipper in three distinct stages. *Science* **337**, 1340–1343 (2012).
17. A. West, K. Ma, J. L. Chung, J. T. Kindt, Simulation studies of structure and edge tension of lipid bilayer edges: Effects of tail structure and force-field. *J. Phys. Chem. A* **117**, 7114–7123 (2013).
18. H. J. Risselada *et al*., Line-tension controlled mechanism for influenza fusion. *PLoS One* **7**, e38302 (2012).
19. M. D'Agostino, H. J. Risselada, L. J. Endter, V. Comte-Miserez, A. Mayer, SNARE-mediated membrane fusion arrests at pore expansion to regulate the volume of an organelle. *EMBO J.* **37**, e99193 (2018).
20. H. A. Kramers, Brownian motion in a field of force and the diffusion model of chemical reactions. *Physica* **7**, 284–304 (1940).
21. P. Hanggi, P. Talkner, M. Borkovec, Reaction-rate theory—50 years after Kramers. *Rev. Mod. Phys.* **62**, 251–341 (1990).
22. E. Evans, Probing the relation between force–lifetime–and chemistry in single molecular bonds. *Annu. Rev. Biophys. Biomol. Struct.* **30**, 105–128 (2001).
23. L. Shi *et al*., SNARE proteins: One to fuse and three to keep the nascent fusion pore open. *Science* **335**, 1355–1359 (2012).
24. G. van den Bogaart *et al*., One SNARE complex is sufficient for membrane fusion. *Nat. Struct. Mol. Biol.* **17**, 358–364 (2010).
25. R. Mohrmann, H. de Wit, M. Verhage, E. Neher, J. B. Sørensen, Fast vesicle fusion in living cells requires at least three SNARE complexes. *Science* **330**, 502–505 (2010).
26. Y. Hua, R. H. Scheller, Three SNARE complexes cooperate to mediate membrane fusion. *Proc. Natl. Acad. Sci. U.S.A.* **98**, 8065–8070 (2001).
27. T. C. Südhof, Neurotransmitter release: The last millisecond in the life of a synaptic vesicle. *Neuron* **80**, 675–690 (2013).
28. F. Manca *et al*., SNARE machinery is optimized for ultrafast fusion. *Proc. Natl. Acad. Sci. U.S.A.* **116**, 2435–2442 (2019).
29. X. Li *et al*., Symmetrical organization of proteins under docked synaptic vesicles. *FEBS Lett.* **593**, 144–153 (2019).
30. P. Heo, F. Pincet, Freezing and piercing of in vitro asymmetric plasma membrane by α-synuclein. *Commun. Biol.* **3**, 148 (2020).
31. T. J. Melia *et al*., Regulation of membrane fusion by the membrane-proximal coil of the t-SNARE during zippering of SNAREpins. *J. Cell Biol.* **158**, 929–940 (2002).
32. P. Heo *et al*., A chemical controller of SNARE-driven membrane fusion that primes vesicles for Ca^{2+}-triggered millisecond exocytosis. *J. Am. Chem. Soc.* **138**, 4512–4521 (2016).